Multiscale Field Theory for Network Flows

Guram Mikaberidze,[1,2] Oriol Artime,[3,4,5] Albert Díaz-Guilera,[3,4] and Raissa M. D'Souza[6,7,8]

[1]*Department of Mathematics, University of California, Davis, California, 95616, USA*
[2]*School of Computing, University of Wyoming, Laramie, Wyoming 82072, USA*
[3]*Departament de Física de la Matèria Condensada, Universitat de Barcelona, 08028 Barcelona, Spain*
[4]*Universitat de Barcelona Institute of Complex Systems (UBICS), Universitat de Barcelona, 08028 Barcelona, Spain*
[5]*Universitat de les Illes Balears, 07122 Palma, Spain*
[6]*Department of Computer Science and Department of Mechanical and Aerospace Engineering, University of California, Davis, California 95616, USA*
[7]*Santa Fe Institute, 1399 Hyde Park Road, Santa Fe, New Mexico 87501, USA*
[8]*Complexity Sciences Hub Vienna, Metternichgasse 8, 1030, Vienna, Austria*

(Received 2 October 2024; accepted 4 April 2025; published 7 May 2025)

Network flows are pervasive, including the movement of people, transportation of goods, transmission of energy, and dissemination of information; they occur on a range of empirical interconnected systems, from designed infrastructure to naturally evolved networks. Despite the broad spectrum of applications, because of their domain-specific nature and the inherent analytic complexity, a comprehensive theory of network flows is lacking. We introduce a unifying treatment for network flows that considers the fundamental properties of packet symmetries, conservation laws, and routing strategies. For example, electrons in power grids possess interchangeability symmetry, unlike packages sent by postal mail, which are distinguishable. Likewise, packets can be conserved, such as cars in road networks, or dissipated, such as Internet packets that time out. We introduce a hierarchy of analytical field-theoretic approaches to capture the different scales of complexity required. Mean-field analysis uncovers the nature of the transition through which flow becomes unsustainable upon unchecked growth of demand. Mesoscopic field theory accurately accounts for complicated network structures, packet symmetries, and conservation laws and yet is capable of admitting closed-form solutions. Finally, the full-scale field theory allows us to study routing strategies ranging from random diffusion to shortest path. Our theoretical results indicate that flow bottlenecks tend to be near sources for interchangeable packets and near sinks for distinguishable ones, and that dissipation hinders the maximum sustainable throughput for interchangeable packets but can enhance throughput for distinguishable packets. Finally, we showcase the flexibility of our multiscale theory by applying it in two distinct domains of road networks and the *C. elegans* neuronal network. Our work paves the way for a more unifying and comprehensive theory of network flows.

DOI: 10.1103/PhysRevX.15.021044

Subject Areas: Complex Systems, Interdisciplinary Physics

I. INTRODUCTION

Complex networks are ubiquitous across a broad range of scales, from cells to societies [1]. Irrespective of their specific domain, these networks consistently contend with the challenge of managing the distribution of matter, energy, and information among their nodes and links [2,3]. We call these types of processes complex network flows. Examples of such flows abound, ranging from neurotransmitters within the brain [4] and individuals within transportation networks [5] to energy transmission in power grids [6] and data packets on the Internet [7]. The proper functioning of these networks relies on their ability to facilitate and sustain flow. However, disruptions can occur for diverse reasons, encompassing overload conditions, intrinsic network malfunctions, or external malicious interventions [8]. Such deviations often pose threats to or halt the operation of the network, exerting adverse impacts on public health, social processes, logistics, and the economy [9–12].

On this basis, there has been broad interest in understanding the conditions under which a network jams, how to quantify the level of congestion, and how to formulate effective responses to these collapses. Given the complex nature of the problem, conventional modeling approaches often resort to computer simulations that are domain

specific, each one with its own nuances and assumptions. The topics investigated mainly amount to the type of network topology the flow unfolds on [13–21] and the routing strategy the packets follow and how they interact [14–17,21–32]. This domain-oriented nature of the problem makes it challenging to develop overarching theories able to establish clear cause-and-effect relationships that are applicable universally across different domains. Similar considerations stem from applied mathematics works, where each network flow problem (e.g., traffic flow on roads, gas dynamics in pipelines, product flow in supply chains, blood circulatory systems, among others) is modeled with its own differential equation, which depends on the particularities of the problem; see, e.g., Refs. [33–35] for reviews.

To bridge this gap, here we take a statistical physics standpoint and categorize network flow phenomena based on their conceptual similarities and propose a flexible, unifying mathematical framework for them. The classification boils down to the symmetries and conservation laws of the flowing packets [36]. For example, consider interchangeability symmetry, which means packets are indistinguishable from one another as in sediment particles flowing in river networks [37] or tunneling electrons in charge transport in nanoparticle networks [38,39]. In contrast, packages sent via postal mail are distinguishable and lack interchangeability symmetry. With respect to conservation laws, individual units (e.g., automobiles) in transportation networks are conserved, as opposed to the Internet where data packets self-delete once they time out. Notably, in addition to the different packet symmetries and conservation laws, our framework also accounts for packet origin-destination distributions and routing strategies. It relies on a multiscale hierarchy of field-theoretic models that offers insights at the macroscopic, mesoscopic, and microscopic description levels. We refer to our approach as a "multiscale field theory" because we aggregate discrete packets into continuous fields at different levels of coarse-graining on the network and systematically derive the time evolution of the fields. The increased resolution allows higher accuracy and flexibility in the modeling of more aspects of the dynamics, although this comes at the expense of more complicated mathematical treatments. To the best of our knowledge, this work is the first inherently multiscale characterization of flows on networks with varied symmetries, conservation laws, and navigation schemes.

Beyond the fundamental interest in the unifying mathematical description of network flows, the deployment of our theory allows us to significantly advance the state of the art and to unravel a set of results of particular relevance. For instance, all the hierarchical levels of our analytical work predict that the flow sustainability will abruptly collapse upon unchecked growth of demand, resembling the behavior observed in empirical systems, where such a transition can manifest in different ways, such as cascading failures or jams. Additionally, the mesoscopic and full-scale approaches offer the possibility of including in the analyses relevant structural properties such as the distribution of the degrees and their correlations (assortativity and others [40,41]), shortest paths, and closed loops of arbitrary lengths. Thus, we are not limited to the restricted regime of treelike structure that pervades many network models, and yet we are capable of providing closed-form solutions, facilitating an efficient exploration of flows on structures that display topological correlations. A nontrivial effect of packet dissipation is also unveiled, and we explain when and why it can help maximize throughput. Finally, we are able to give insights about where the flow bottlenecks begin developing given the symmetries of the flow, as well as in which regimes the routing randomness collapses the system. All these results are derived under minimal assumptions, hence offering a solid backbone on which one can easily tailor to more constricted network flow models that need to capture domain-oriented specificities.

The rest of the article is organized as follows. In Sec. II A, we formulate the specific rules of network flow dynamics, incorporating symmetries and conservations. In Secs. II B–II D, the mean-field, mesoscopic, and full-scale field theories are, respectively, derived. In Sec. III, we discuss the results and implications of each level of analytic treatment. Finally, in Sec. IV, we give the summary and conclusions.

II. MODEL AND METHODS

In this section, we present our hierarchy of field-theoretic approaches to tackle flow distribution and jamming transitions on networks. The models will be introduced in an increasing level of intricacy, from the most coarse-grained description to the most fine-grained one.

A. General considerations

We define a packet as the discretized minimal amount of any physical or informational quantity that is spreading over the edges of a network. The goal of our minimal models is to incorporate the effects of packet conservation or dissipation and interchangeability or distinguishability on the global dynamics of the flow, as well as the routing strategies the packets use to navigate the network. In addition, we keep the system as simple as possible, but it can be extended to incorporate various detailed properties for specific real-world applications. The dynamics is described by the following steps:

(1) Packets are generated at the rate g_i on node i, $\forall\ i \in \{1, \ldots, N\}$.
(2) The origin nodes where the packets are created are called the sources, and the destination nodes where the packets are removed are called the sinks. The packet navigates the network until reaching an appropriate sink via some routing strategy.
(3) Packets can leave the system if they are dissipated (deleted) with probability ϵ when flowing or if they successfully reach their destination.

The flow is conservative when $\epsilon = 0$ and dissipative when $0 < \epsilon \leq 1$. Whenever a source generates a packet, a corresponding sink label is generated by some other node in the network, indicating that the node is expecting a packet. This case is similar to modeling power grid networks, where some nodes are designated as sources and others as sinks. Notice that, in our model, a node may be labeled as a sink by multiple packets, but each packet that the sink absorbs will only erase one label. If the packets are distinguishable, sinks will absorb only packets generated by their counterpart sources. In this case, all nodes can potentially be sources and sinks, similar to packages sent on postal networks. If, in contrast, the packets are interchangeable, sink nodes will absorb any packet that reaches it. Thus, at any time, there are as many source-sink pairs as there are packets present on the network.

For the sake of simplicity, we assume throughout that the generation rate is independent of the nodes, i.e., $g_i = g, \ \forall \ i$, and that each edge can conduct at most one packet per iteration. These assumptions can be easily relaxed in the mathematical treatment and in the numerical experiments. Moreover, time is considered discrete, and the position of all the packets is updated simultaneously, conditioned on the finite capacity of edges per iteration. In other words, each packet simultaneously chooses an edge to attempt to move through, and if one edge is chosen by multiple packets, then only one of the packets, selected at random, is actually transported across the edge while the others remain stuck on the original node. The packets will navigate the network following various routing strategies, from those based on local information, such as random-walk-like movements, to those incorporating global network data, such as shortest-path routing. Furthermore, our theory allows us to interpolate between these two extreme routing cases continuously.

The dynamics can be implemented either on directed or undirected networks. For the sake of clarity, we focus on undirected networks, and edges will be bidirectional, conducting at most one packet in each direction. Thus, an undirected network with E edges will be equivalent to a directed network with $2E$ edges, each bidirectional edge replaced with two directed edges. This equivalence will be used later to simplify notation in derivations. It should be noted that when we do not explicitly mention directed edges, we always mean an undirected edge.

We write down equations describing the temporal evolution of the number of packets $s(t)$ present in the system at time t. One of the metrics we consider, mathematically and computationally, to characterize the flow is the throughput (or flux) F, i.e., the number of packets that reach their destinations per iteration. We are also interested in the critical generation rate g_c, i.e., the maximum number of packets that can be input into the network without jamming it.

Our approach here is more general than, and differs from, the scarce analytical works that have previously tackled the problem of network flows. In the physics literature, one can mainly find, according to our multiscale classification, mean-field approximations. For instance, in Ref. [25], Martino *et al.* consider the conservative flow of distinguishable packets under two distinct routing strategies, and they establish the continuous and discontinuous emergence of congestion. In Ref. [26], Wang *et al.* discuss a similar model for a family of local routing strategies that incorporate dissipation, and through a mean-field analysis, they provide a qualitative description of the flow congestion. Other works [14,21] analytically study the conservative flow of distinguishable packets for arbitrary routing strategies in the so-called microscopic congestion model, which is based on the algorithmic betweenness of each node. Our model contributes new conceptual classes of flow phenomena in some cases (e.g., for indistinguishable packets) and enriches the analysis with quantitative evaluations where prior studies offer primarily qualitative insights (e.g., dissipative flows). Another significant difference in our approach lies in the way we implement the limitations on the flow. All the models above consider the flow rates to be limited by the nodes, and the edges impose no constraints. In contrast, in our approach, this limitation is surmounted, and the finite conductive capabilities of the edges are taken into account, thus extending the possibility to better describe real flows.

B. Mean-field theory

To set the stage, let us start our analysis with the simplest approach, namely, a mean-field theory of the flow. Parts of this derivation will be useful in later sections as well. In this approach, we disregard the correlation between neighbor nodes; i.e., all nodes are treated on equal footing, and each edge is assumed to lead to any other node in the network with equal probability. Effectively, this approach is equivalent to considering all-to-all connectivity. We first analyze the random-walk routing of distinguishable packets.

We assume an arbitrary network of N nodes and E undirected edges. At time t, the system contains $s(t)$ packets, all of which are attempting to pass through the total number of $2E$ directed edges. Some of the packets will successfully make the jump across an edge, while others will be stalled if the directed edge they selected is occupied. To find the total flow, i.e., the number of packets that moved successfully, let us consider the probability that one directed edge remains available throughout a single iteration. Because of the mean-field assumption, each packet selects one directed edge uniformly at random. Thus, the probability of a specific packet selecting a specific directed edge is $(1/2E)$. The probability of this selection not happening is $[1 - (1/2E)]$, and a directed edge will remain free throughout the iteration if all the $s(t)$ packets select some other directed edge, which happens with probability $[1 - (1/2E)]^{s(t)}$. Thus, the expected number of occupied directed edges is $2E\{1 - [1 - (1/2E)]^{s(t)}\}$. Since each of these directed edges conducts exactly one packet, this

number is also the expected amount of the total flow. In summary, when s packets are attempting to flow through d_e directed edges, the expected net flow is

$$f(d_e, s) = d_e\left[1 - \left(1 - \frac{1}{d_e}\right)^s\right]. \tag{1}$$

The concept of expected net flow will also appear in the other hierarchical levels of our field theory, and, accordingly, Eq. (1) will be used in their mathematical descriptions as well.

An ϵ fraction of this flow will be dissipated and, because of the mean-field assumption, $1/N$ fraction of the remaining packets will reach their destinations. Thus, the time-dependent throughput in the mean-field description reads

$$F(t) = \frac{1-\epsilon}{N} f\big(2E, s(t)\big). \tag{2}$$

With the expressions for the flow and throughput, we can now write down the dynamical equation for $s(t)$, namely,

$$\begin{aligned}\frac{\mathrm{d}s(t)}{\mathrm{d}t} &= -\frac{1-\epsilon}{N} f\big(2E, s(t)\big) - \epsilon f\big(2E, s(t)\big) + gN \\ &= -(1-\epsilon+\epsilon N)\frac{2E}{N}\left[1 - \left(1 - \frac{1}{2E}\right)^{s(t)}\right] + gN. \end{aligned} \tag{3}$$

This formula is a gain-loss equation, where the first term on the right-hand side accounts for packets leaving the system via throughput and the second term via dissipation. Both of these terms are proportional to the net amount of flow. The third term is the gain, accounting for the packets that are added to the system through the sources. Here, g is the packet generation rate per node.

In order for the flow to be sustainable on a given network, Eq. (3) must have a stationary state solution, i.e., $(\mathrm{d}s/\mathrm{d}t) = 0$. In the stationary state s^*, we can rearrange the equation into

$$1 - \frac{gN^2}{(1-\epsilon+\epsilon N)2E} = \left(1 - \frac{1}{2E}\right)^{s^*}. \tag{4}$$

Notice that the right-hand side of the equation is nonnegative, yet if one increases the generation rate g beyond some critical value g_c, the left-hand side will become negative. Thus, for large enough generation rates, the dynamics has no stationary state, and the total number of packets in the network grows indefinitely, This state is commonly called a congested or jammed state. The flow will be sustainable only for bounded generation rates $g < g_c$. The g_c at which the jam emerges can be expressed as

$$g_c = \frac{(1-\epsilon+\epsilon N)2E}{N^2}. \tag{5}$$

When the sustainability condition $g < g_c$ holds, we can use Eq. (4) with Eq. (2) to express the stationary value of the throughput,

$$F = gN\frac{1-\epsilon}{1-\epsilon-\epsilon N}\Theta(g_c - g), \tag{6}$$

where $\Theta(x)$ is the Heaviside step function. We have included it in the throughput expression in order to explicitly account for the eventual system failure when the flow is unsustainable.

To finish the mathematical derivations of this section, we motivate our choice behind the quantities we employ to characterize the flow and its congestion. An order parameter used previously in the literature to study jamming phase transitions reads

$$\eta(g) = \lim_{t\to\infty}\frac{1}{gN}\frac{\mathrm{d}s(t)}{\mathrm{d}t}, \tag{7}$$

which measures the fraction of the generated packets retained by the system in the asymptotic state [21,25]. As the generation rate g becomes larger than g_c, the stationary state disappears, the system starts to accumulate packets, and η becomes nonzero. However, η does not account for dissipation, so it is not an appropriate observable for our purposes since dissipation introduces a new way for packets to exit the system without contributing to the throughput. As an extreme example, consider the dissipation rate $\epsilon = 1$, which has corresponding $\eta = 0$ since no packets accumulate, indicating good performance but missing the fact that the throughput is zero. Thus, we focus on the sustainable throughput F, which is a more relevant variable from a practical perspective when different symmetries and conservation laws are at play.

Figure 1 shows the comparison of the mean-field theoretic analysis with simulated data on random regular networks, i.e., homogeneous networks in which all nodes have the same number of neighbors, chosen uniformly at random [42]. For dense networks [see Fig. 1(a)], simulations confirm the analytic results. However, when networks are more sparse, the mismatch becomes tangible [see Fig. 1(b)] because of the core assumption of the mean-field theoretic approach—namely, the disregarded correlations become important. For large, sparse networks, a packet has to travel far to reach the destination, and the probability of discovering a packet in a specific node changes significantly with the distance to the sink. Still, the qualitative behavior of the system remains accurate for sparse networks.

In the following subsection, we develop a more detailed mesoscopic field theoretic analysis of the system that accounts for arbitrary network structures. We also further clarify the reasons leading to the failure of the mean-field approach for sparse networks.

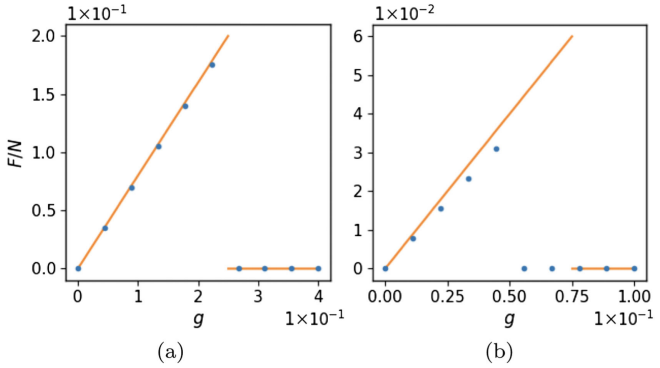

FIG. 1. Comparison between the mean-field treatment and numerical simulations. We show the stationary throughput per node F/N as a function of generation rate g. Initially, increasing g increases the number of packets and, subsequently, the throughput. However, beyond the critical value $g \geq g_c$, the flow becomes unsustainable, and the system jams, represented here as $F = 0$. The considered topologies are random regular networks of size $N = 50$ with density 0.2 (a) and with density 0.06 (b). Dissipation is set to $\epsilon = 0.005$. The solid line corresponds to Eq. (5). The markers correspond to simulations, averaged over eight independent realizations, and error bars, too small to see, indicate the standard error. The mean-field theory is less accurate if networks are very sparse.

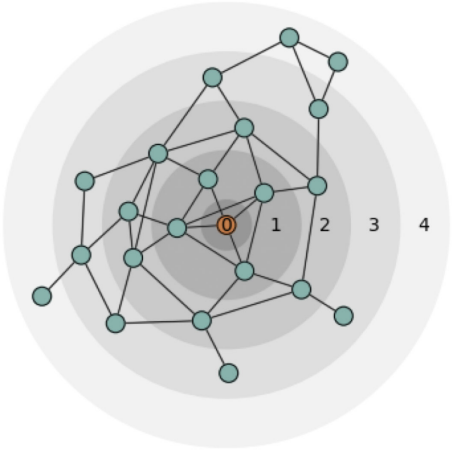

Layer r	0	1	2	3	4
N_r	1	4	7	7	3
E_r	0	4	8	9	4
D_r	4	20	33	17	6

FIG. 2. Network profile as seen from the perspective of the node in layer 0. A network has as many profiles as it has nodes, but the mesoscopic theoretic approach aggregates them as a function of the degree of the central node. Hence, we reduce the description of the system from N to $d_{\max}$ variables, where N and $d_{\max}$ are the network size and the maximum degree, respectively. On the bottom, we report a table with the main quantities used in the theory (see Sec. II C) for this particular network profile. Note that N_r is the number of nodes in layer r, E_r is the number of interlayer edges between $r-1$ and r, and D_r is the sum of node degrees within layer r.

C. Mesoscopic field theory

Inspired by the theory of statistical physics and critical phenomena, the main idea behind the mesoscopic field-theoretic approach is to identify which are the most relevant traits of the network topology that are able to explain the key characteristics of the flow. To do so, let us first consider the network as seen from the perspective of a single node. We refer to this node as the center, and the important aspects of the network topology, from the perspective of the given center, will be called the network profile. The profiles will enable us to aggregate nodes by their similarities in terms of how they contribute to the flow properties. Network profiles are intimately related to the concept of network portraits [43], but they contain more structural information and are defined at the node level instead of the node degree level.

The network profile is organized in concentric layers around a center node according to hop distance as shown in Fig. 2. Neighbors of the center node will belong to the first layer, nodes two hops away from the center will be in the second layer, and so on. In the context of a given profile, let us denote by N_r the number of nodes in layer r, by E_r the number of undirected edges connecting layers $(r-1)$ and r, and by D_r the sum of node degrees within layer r. The boundary conditions are $E_0 = E_{R'+1} = 0$, where R' is the index of the last layer for that particular profile. In this way, we are grouping all the N_r nodes in each layer r into a single aggregated location, situated r hops away from the center. The structural parameters E_r tell us how well these aggregated locations are interconnected. On the other hand, D_r simultaneously holds the information about the intralayer and interlayer connectivity. For illustrative purposes, in the table within Fig. 2, we report the values (N_r, E_r, D_r) for the particular network profile shown. Moreover, if nodes have any attributes relevant to the dynamics, such as being designated sources, sinks, or something completely different for an alternative application of the framework, we also keep track of the attribute distributions in each layer. This aggregated structural information is the network profile, as seen from a specific center. The structural parameters composing the profile are the building blocks of our mesoscopic framework. Profiles can be computed numerically for a specific network or analytically from the degree distribution of the configuration model. Details on the latter will be given below.

The computation of the network profiles for each node in the role of the center yields N profiles, each with at most R aggregated locations, where R is the network diameter. We could start modeling the dynamics at this point, but first we perform a significant simplification that reduces the degrees of freedom by grouping the profiles by some similarity measure and only considering a single representative profile from each group.

Here, we proceed heuristically by using the simplest centrality score of nodes, i.e., their number of connections. Indeed, grouping the profiles by the degree of the central node turns out to be a good strategy. This method produces at most $d_{\max}$ groups, where $d_{\max}$ denotes the maximum degree. Hence, the upper bound of the number of aggregated locations is reduced to $(R \times d_{\max})$ representative aggregated locations. Since both real-world and uncorrelated synthetic networks are usually sparse with $d_{\max} \ll N$ [44], the reduction in the degrees of freedom that we need to keep track of is considerable. It should be mentioned that grouping by degree is not the only possibility, especially for the cases with heavy-tail degree distributions where the degrees can become extremely high. Other alternatives include grouping by the k-core structure [45] or using machine-learning tools like k-means clustering directly on the profile data [46].

We number the similarity groups by α, and for each group α, we compute a representative profile $(N_r^\alpha, E_r^\alpha, D_r^\alpha)$ by simply averaging all profiles in the α group. Alongside the averages, we keep track of the similarity group sizes w^α, i.e., the weight by which each representative profile affects the dynamics. Finally, we can model the dynamics over these representative aggregated locations. The details of exactly how the dynamical models are constructed depend on the symmetries of the system; therefore, in the following, we will consider the cases of distinguishable and interchangeable packets separately.

1. Distinguishable packets

In this section, we study the flow of distinguishable packets under random-walk routing. For each representative profile α, we keep track of all the packets s_r^α that have the center as their destination. The subscript r indicates that we keep the count of such packets in each layer separately. In other words, we consider the flow of relevant packets from the perspective of the sink nodes. The total number of packets targeting the center of the α profile is given by $\sum_r s_r^\alpha$ and, since there are w^α such profiles, the total number of packets in the system is

$$S = \sum_{\alpha,r} w^\alpha s_r^\alpha. \tag{8}$$

We aim to set up dynamical equations for the variables s_r^α. These variables change in time due to the packet generation and absorption, the inflow from and outflow to neighbor layers, and the dissipation from internal flows. The dissipation also acts on interlayer flows, resulting in a mismatch between outflows and inflows.

Random-walk routing implies that, during each iteration, each packet chooses a neighbor node uniformly at random and attempts to jump to it. Here, $P_{\alpha,r}^{\text{in}}$, $P_{\alpha,r}^{\text{loc}}$, and $P_{\alpha,r}^{\text{out}}$ denote the probabilities that a packet in the layer r of profile α will attempt the jump to the inner layer, within the current layer, or to the outer layer, respectively. For $r > 0$, these probabilities can be calculated based on the profile information:

$$\begin{aligned} P_{\alpha,r}^{\text{in}} &= \frac{E_r^\alpha}{D_r^\alpha}, \\ P_{\alpha,r}^{\text{loc}} &= \frac{D_r^\alpha - E_r^\alpha - E_{r+1}^\alpha}{D_r^\alpha}, \\ P_{\alpha,r}^{\text{out}} &= \frac{E_{r+1}^\alpha}{D_r^\alpha}. \end{aligned} \tag{9}$$

At the center of the profile, $r = 0$, the packets s_0^α have already reached their destination, and they do not attempt any further jumps. This case is mathematically expressed as $P_{\alpha,0}^{\text{in}} = P_{\alpha,0}^{\text{loc}} = P_{\alpha,0}^{\text{out}} = 0$.

We can now write the dynamical equations for the number of packets s_r^α,

$$\begin{aligned} \frac{\mathrm{d}s_r^\alpha}{\mathrm{d}t} = &-\delta_{0r} s_r^\alpha + (1-\delta_{0r}) N_r^\alpha \frac{g}{N-1} + s_{r-1}^\alpha P_{\alpha,r-1}^{\text{out}} v(1-\epsilon) \\ &+ s_{r+1}^\alpha P_{\alpha,r+1}^{\text{in}} v(1-\epsilon) - s_r^\alpha (P_{\alpha,r}^{\text{in}} + P_{\alpha,r}^{\text{out}}) v - s_r^\alpha P_{\alpha,r}^{\text{loc}} v\epsilon. \end{aligned} \tag{10}$$

The first term on the right-hand side accounts for the packet absorption by the sink, which happens only at the center $r = 0$, the condition enforced by the Kronecker delta δ_{0r}. The second term is a gain contribution due to sources, with g denoting the packet generation rate per node and with the factor $(1 - \delta_{0r})$ ensuring that packets are not generated with the same destination as the source. The full generated number of packets is proportional to the number of nodes in the layer N_r^α, and each generated packet has a random destination among $(N-1)$ remaining nodes, one of which is the center of the profile α. The third and fourth terms account for the inflow of packets from the neighboring layers $(r-1)$ and $(r+1)$. For example, $s_{r-1}^\alpha P_{\alpha,r-1}^{\text{out}}$ is the expected number of packets from the inner layer that attempt to jump to layer r. The variable v denotes the flow rate of packets: It is 1 when packets are few and not interacting, and tends to 0 in jammed states. Thus, a fraction v of all these packets will find an available edge, so a further fraction $(1-\epsilon)$ will survive the dissipation, amounting to $s_{r-1}^\alpha P_{\alpha,r-1}^{\text{out}} v(1-\epsilon)$. The fifth term accounts for the outflow to the neighboring layers, while the last term is the dissipation due to the intralayer flow.

The index $\alpha \in \{0, 1, \ldots, m\}$ enumerates the representative profiles, while $r \in \{0, 1, \ldots, R^\alpha\}$ enumerates the layers of the α profile, where R^α is the radius of the profile. Therefore, we have one such equation, Eq. (10), for each profile α and each layer r, with the number of equations bounded above by $(R \times d_{\max})$, with $d_{\max}$ standing for the maximum degree and R denoting the diameter of the network [note that $R = \max_\alpha(R^\alpha)$].

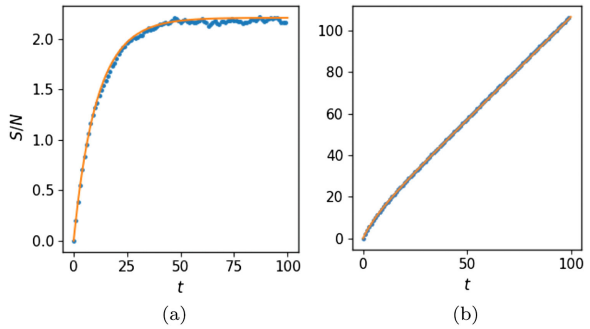

FIG. 3. Comparison between theory and simulations for distinguishable packets under random-walk routing. We show the packet density (S/N) as a function of time t in Erdős–Rényi graphs with $N = 1000$ nodes and $E = 5000$ edges. The generation rates are $g = 0.2$ (a) and $g = 2$ (b). Dissipation is $\epsilon = 0.1$. Markers correspond to simulations, while the orange solid curves come from the numerical integration of mesoscopic field-theoretic equations (10). For low values of generation rate g, the total amount of packets becomes saturated, and the system reaches a stationary state (a). Meanwhile, for large values of g, the stationary state is never reached, and the total number of packets diverges to infinity (b). Each plot corresponds to data from a single simulation, highlighting the fact that our theoretical predictions can not only accurately capture ensemble averages but also the flow properties from individual realizations of the dynamics.

We need to calculate the average flow rate v, i.e., the fraction of all packets that successfully moved. Employing Eq. (1), we obtain

$$v = \frac{1}{S} f(2E, S) = \frac{2E}{S}\left[1 - \left(1 - \frac{1}{2E}\right)^{S}\right]. \qquad (11)$$

Here, E is the number of edges, and S is the total number of packets in the system. Note that, for simplicity, we compute the average value of the flow rate in the full system, which is based on the assumption that the packets from other profiles tend to jam the edges in the given profile uniformly at a globally computed rate. This assumption implies that the profiles are uncorrelated; i.e., edges from one profile are uniformly distributed in another profile. However, the equations remain precise for highly correlated networks. Nonetheless, one could lift the assumption of profile independence by keeping track of profile correlations, albeit this would result in much more complicated equations.

We verify the performance of Eq. (10) by numerically integrating it and comparing it to simulated data. In Fig. 3, we show the time dependence of the total number of packets in the system for low [$g = 0.2$, Fig. 3(a)] and high [$g = 2$, Fig. 3(b)] generation rates. The computations are done for networks with edge density 0.01, which are much sparser than the network for which the mean-field approach failed in Fig. 1. This case indicates that the issues of the mean-field approach are avoided in the mesoscopic treatment.

Inspecting the network load time series in more detail, we notice that, in the congested phase [Fig. 3(b)], $S(t)$ increases linearly over time without noticeable fluctuations. In the jammed state, the load accumulates faster than it can exit the system, leading to a steady buildup of packets in the nodes. Since each edge has a fixed, finite conductive capacity, the throughput is also finite and bounded above, leading to vanishing relative fluctuations in $S(t)$. This finding also means that the probability of any specific packet being repeatedly selected to jump through the links and reach its destination becomes vanishingly small. From a specific packet perspective, the network becomes untraversable. In contrast, fluctuations in $S(t)$ are indeed observed in the free-flow regime [Fig. 3(a)]. Thanks to the analytical model provided here, we can differentiate the two regimes and accurately predict the jamming point. In the absence of such a model, analyzing the statistical properties of these fluctuations serves to infer how close the system is to the jamming transition [47].

The complicated nature of the dynamics in Eq. (10) stems from the nonlinear interactions of packets in the edges, encoded through the appearance of the total number of packets S in the expression of the flow rate v, as seen in Eq. (11). Despite of this nonlinearity, relevant analytical insights can be obtained. Looking at the stationary state, we can find the optimal stationary operation regime of such flows. From the mean-field theoretic analysis, we see that the throughput initially increases as a function of g, until a point $g > g_c$ where the flow becomes unsustainable. Thus, we expect the optimal generation rate to be the value right before this transition. As g approaches g_c from below, the stationary number of packets increases, until it finally diverges at $g = g_c$. Then, at the transition, we can use $S \gg 1$ to simplify the flow rate in Eq. (11) significantly, resulting in $v = (2E/S)$. Intuitively, right before the transition to the jammed state, the system utilizes its conduction capability to the maximum extent. Still, we have nonlinear couplings in the system since $S = \sum_{\alpha,r} w^{\alpha} s_r^{\alpha}$, which can be remedied by a change of variables

$$s_0^{\alpha} \to s_0^{\alpha}, \quad \text{and} \quad s_r^{\alpha} \to \frac{s_r^{\alpha}}{S} \quad \text{for } r \geq 1. \qquad (12)$$

In addition, we treat the generation rate $g = g_c$ as a variable and add Eq. (8) as the last entry to the system of equations (10), which results in a linear system of the form $\boldsymbol{A} \cdot \boldsymbol{x} = \boldsymbol{e}$. The explicit expressions for $\boldsymbol{A}$, $\boldsymbol{x}$, and $\boldsymbol{e}$ are given in Appendix B.

The complexity of the mesoscopic description of the flow problem has been reduced to solving a linear matrix equation. The solution $\boldsymbol{x} = \boldsymbol{A}^{-1} \cdot \boldsymbol{e}$ contains the critical generation rate g_c, all the information regarding the number of packets in every layer and in every profile, and,

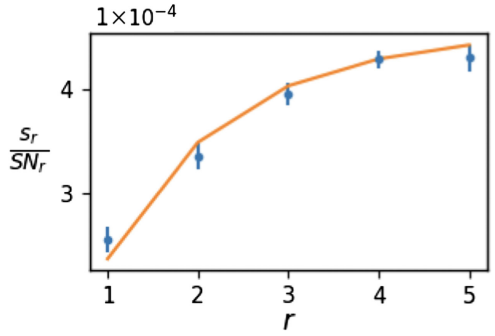

FIG. 4. Radial location of the packets. We display the fractional density of packets (s_r/SN_r) as a function of layer index r, i.e., the probability of finding a packet in a specific node distance r away from its destination. Computations are performed for distinguishable packets, under random-walk routing, on a random three-regular network of $N = 50$ nodes with generation rate $g = 0.032$ and dissipation probability $\epsilon = 0$. Since all nodes have identical degree, we only consider one network profile; hence, the superscript α is absent from s_r^α. Blue data points show the mean of 16 independent realizations, and the error bars show the standard error. The orange curve comes from mesoscopic field theoretic analysis in Eq. (B2), and the interpolation to noninteger values of r is performed for visual appeal.

therefore, the total amount of throughput $F = \sum_\alpha w^\alpha s_0^\alpha$. The analytical expressions for the solutions become cumbersome and not very enlightening, yet we highlight that we have arrived at a closed-form solution that can be evaluated in a very quick and efficient manner via matrix inversion. Indeed, the square matrix $\boldsymbol{A}$ has a single dimension for each layer of each representative profile, plus one for the generation rate. Then, as discussed before, the matrix size is bounded above by $R \times d_{\max} + 1$, and the time complexity of its inversion will be bounded above by $\mathcal{O}((R \times d_{\max})^3)$ (we assume cubic complexity of inversion with respect to matrix size, but we should note that there are asymptotically faster algorithms that become practical for very large matrices).

We can use this solution to look deeper into the reasons why the mean-field approach fails to work as expected and exactly how the mesoscopic field theory resolves the issue. In Fig. 4, we display the fractional density of packets (s_r/SN_r) for various layers r in the stationary state. In other words, the figure shows the probability of finding a packet in a specific node as a function of the distance r between the node and the destination. Figure 4 indicates that the probability of finding a packet in a specific node becomes significantly higher as the distance from the destination increases. This clearly important feature is fully neglected by the mean-field approach and well accounted for by the mesoscopic approach.

2. Interchangeable packets

Let us turn to the scenario of interchangeable (i.e., indistinguishable) packets. In this case, a packet is deleted upon its arrival to any sink, regardless of the original sink label that was associated with its creation. Therefore, unlike the distinguishable case, where we aggregated the packets with the same sink destination into one field, all the packets will now make up a single field.

As discussed above, similar to how power-grid dynamics are modeled, we must assign distinct roles to nodes: designated (i.e., potential) source nodes and designated (potential) sink nodes. Then, during the profile computations, we keep track of the prevalence of each of these node attributes in the layers. Let us denote the number of designated source and sink nodes in layer r by O_r and I_r, respectively. A similar origin-destination node splitting approach is used in transition path theory from computational chemistry [48]. However, in that context, it is assumed that complete information about the set of nodes, links, and link weights is available in advance, whereas in our case, this assumption is not required.

We find that, to ensure the accuracy of the model, in the scenario of interchangeable packets, the profile centers must be associated with the sources, contrary to the distinguishable scenario, where they were selected to be sinks. This requirement suggests that the bottlenecks of the flow now occur near the sources. We will explore the reasons and implications of the necessity of this change in Sec. III.

Following similar arguments as in the previous section, we can now write down the dynamical equations for $s_r(t)$ in a single profile:

$$\begin{aligned}\frac{\mathrm{d}s_r}{\mathrm{d}t} = {} & gO_r + \left[f(E_r, s_{r-1}P_{r-1}^{\mathrm{out}}) + f(E_{r+1}, s_{r+1}P_{r+1}^{\mathrm{in}})\right] \\ & \times (1-\epsilon)\frac{N_r - I_r}{N_r} - f(E_r, s_r P_r^{\mathrm{in}}) - f(E_{r+1}, s_r P_r^{\mathrm{out}}) \\ & - f(D_r - E_r - E_{r+1}, s_r P_r^{\mathrm{loc}})\left(\epsilon + (1-\epsilon)\frac{I_r}{N_r}\right). \quad (13)\end{aligned}$$

The first term on the right-hand side is the source (gain). In contrast to Eq. (10), each layer r contains the total number of I_r sinks, and hence (I_r/N_r) fraction of packets arriving at this layer land on sinks. This time, the congestion level is calculated locally for each layer. The $f(\ldots)$ terms on the second, third, and fourth lines account for the inflow from adjacent layers, outflow to adjacent layers, and local flow within the layer, correspondingly. Terms with ϵ account for dissipation, and terms with I_r account for absorption. For example, the term $f(E_r, s_{r-1}P_{r-1}^{\mathrm{out}})$ computes the number of packets from layer $r-1$ that attempt to travel to layer r and successfully secure one of the E_r edges for this jump. Note that $(1-\epsilon)$ accounts for the dissipation during the jump, and $[(N_r - I_r)/(N_r)]$ accounts for the absorption of part of this flow that landed on sinks.

An equation like Eq. (13) can be written down for each profile. Notice, however, that there are no interactions between the equations from different profiles. Each profile

describes the full flow of all the packets, as seen from the perspective of different centers. Therefore, if the flow is unsustainable from the perspective of at least one center, then the flow will automatically be globally unsustainable.

Unfortunately, we could not find a closed-form solution for the steady state in this case. Instead, one can either solve the dynamics using numerical integration techniques such as Runge-Kutta methods or, alternatively, directly find the stationary state using the high-dimensional Newton method with exact or approximate Jacobians [49]. We proceed numerically, always finding excellent accuracy when compared to simulations. To illustrate this point, we show in Sec. III E that Eq. (13) properly characterizes the flow and the jamming transition in an empirical road network.

In the direct approach, we have N profiles with roughly R layers each; thus, we have N systems of roughly R coupled equations. However, this number can be significantly reduced by introducing some heuristics for the bottleneck locations. For example, for interchangeable packets, the bottlenecks occur near large concentrations of source nodes; thus, we only need to consider the profiles centered at the sources or, even better, select a few profiles centered at the highest concentration of sources in the network. These profiles will be the first ones to detect the unsustainability of the flow; hence, if neither of these bottleneck locations predicts unsustainability, the flow will be sustainable. Therefore, if they predict a sustainable flow, all others would also produce the same result.

3. Network profiles

As a final note in this subsection, we remark that the derivations presented in the mesoscopic analyses crucially depend on the topological parameters (N_r, E_r, D_r) and their α-aggregated counterparts. They can be computed numerically for a given network by considering each node as the center and then exploring all the edges step by step, unfolding the structure of the profile radially outward. This procedure has $\mathcal{O}(N \times E)$ time complexity. The profiles then serve as an input to our analytic treatment.

The numerical computation of the profiles, however, does not directly give intuition on how the flow properties depend on the parameters of the network models, such as the mean-degree of Erdős-Rényi graphs, the exponent of the degree in scale-free nets, the rewiring probability in the Watts-Strogatz model, etc. Throughout the paper, we sample multiple instances of networks for each given parameter and average the analytic results for these networks to distill the dependence on the parameter under question. An alternative approach would be computing the expected network profile directly based on the network parameters and performing the analysis for this single true average. This analysis is out of the scope of the current work, but we report in Appendix A, for completeness, analytical approximations for these structural parameters for the configuration model that, if needed, would allow us to address these questions.

D. Full-scale field theory

So far, we have focused on the random routing of both distinguishable and interchangeable packets. Now, we turn our attention to routing strategies that take into account topological information, i.e., those that are not purely random. Employing the relation between randomness and temperature in thermal systems [50], let us introduce here the routing temperature $T \in [0, 1]$ that will interpolate between shortest-path ($T = 0$) and random routing strategies ($T = 1$). At each iteration, each packet will choose a random direction with probability T, or it will follow the shortest path to its destination with probability $1 - T$. Thus, by tuning T from 0 to 1, we can continuously explore the full spectrum of routing strategies between the shortest-path routing and the random walk. The properties of this navigation strategy have been studied in the context of network neuroscience [51], and similar proposals of routing strategies that randomly switch between two flowing modes have recently been proposed in the literature [52]. Furthermore, the concept of temperature T as a parameter that monitors trajectory randomness has been successfully used elsewhere, such as in the bag-of-path framework that was introduced to probabilistically sample network paths fulfilling certain properties [53].

As before, an important consideration lies within the locations of the potential bottlenecks. In the shortest-path routing, the trajectories of multiple packets may well intersect somewhere in the middle of the path. Actually, as observed in our simulations, the bottlenecks are prone to appear near the nodes with high betweenness centrality, independently of their proximity to the sources or the sinks. However, for arbitrary values of T, their locations become hard to predict. Thus, to model the process accurately, we need to keep high-resolution information everywhere in the network. This approach motivates the development of a full-scale field theory, where each node is treated as a separate location, and the edge information is given by the adjacency matrix A_{ij} [42].

Let us start by considering the flow of distinguishable packets. Following previous reasonings, we aggregate the packets with the matching destinations into a single field, which will now be defined over the network nodes. In other words, $s_{ik}(t)$ is the expected number of packets in node i with destination k, at time t.

Modeling the random-walk steps is simply performed using the adjacency matrix A_{ij}. To set up the shortest-path steps, instead, we need to precompute the shortest-path tensor P_{ijk}. Denoting the distance between nodes i and k by L_{ik}, we define the shortest-path tensor as

$$P_{ijk} = \begin{cases} 1 & \text{if } A_{ij} > 0 \quad \text{and} \quad L_{ik} > L_{jk} \\ 0 & \text{otherwise.} \end{cases} \tag{14}$$

In other words, P_{ijk} is 1 if jumping from i to j leads to k, and it is 0 otherwise. This tensor accounts for path multiplicity; i.e., $P_{ij'k} = P_{ij''k} = 1$ if nodes j' and j'' are at the same distance from k. The distances L_{ik} can be computed efficiently using a breadth-first search originating from each of the nodes in $O(N^2)$ time complexity for sparse networks [54]. Since the network structure is unaltered throughout the dynamics, we only need to perform this computation once, as it occurs with the network profiles.

Now, we can calculate the probability that a packet located in node i, and whose destination is node k, will attempt to jump to node j. It reads

$$M_{ijk} = (1-\delta_{ik})\left[T\frac{A_{ij}}{\sum_h A_{ih}} + (1-T)\frac{P_{ijk}}{\sum_h P_{ihk}}\right]. \quad (15)$$

The factor $(1-\delta_{ik})$ ensures that the packets at their destinations will not attempt to jump anywhere. The first term in the square brackets accounts for the random-walk step, which happens with probability T. Note that $[(A_{ij})/(\sum_h A_{ih})]$ is the uniform normalized probability over all the neighbors j. The second term is for the shortest-path jump, occurring with probability $1-T$, and it gives uniform normalized probabilities over the possible shortest-path directions j. The normalization is necessary since there may be multiple shortest paths between i and k with different first steps j.

The expected number of packets attempting to pass through a single edge (i,j) is given by $\sum_k s_{ik}M_{ijk}$. If this value is less than or equal to 1, there will be no congestion in this edge. However, if the value exceeds 1, then only one packet will jump. Thus, the probability that one of these packets will jump successfully—or, alternatively, the average flow rate for all these packets—is given by

$$v_{ij} = \frac{1}{\max\left(1, \sum_h s_{ih}M_{ijh}\right)}. \quad (16)$$

Thus, we can write down the dynamical equations for s_{ik},

$$\frac{\mathrm{d}s_{ik}}{\mathrm{d}t} = -\delta_{ik}s_{ik} + (1-\delta_{ik})\frac{g}{N-1} + \sum_j [s_{jk}M_{jik}v_{ji}(1-\epsilon) - s_{ik}M_{ijk}v_{ij}]. \quad (17)$$

The first two terms account for the sinks and sources. In the sink term, δ_{ik} ensures that packets are absorbed at their destinations. In the source term, g is the packet generation rate per node, and $(1-\delta_{ik})$ guarantees that packets are not generated at their destinations. Each generated packet targets one of the $N-1$ nodes, hence the denominator. The last two terms represent the inflow and outflow from and to all neighbor nodes j.

We note that Eq. (17) is far from linear in s_{ik} due to the nontrivial interactions in the edges seen in the expression for the flow rate, Eq. (16). In total, we have a system of N^2 equations. We were unable to produce a closed-form solution. Instead, one can employ numerical integration techniques to find the evolution of the system in time or utilize the high-dimensional Newton method with approximate Jacobians [49] to find the stationary states directly.

III. RESULTS

The hierarchy of analytic treatments derived in the previous sections provides qualitative insights along with the tools for quantitative predictions. In this section, we apply these tools to explore the flow dynamics under various symmetries and conservations, and we unravel some implications.

A. Jamming transition

The mean-field theory approach neglects all correlations on the network and ignores its structural information beyond the number of nodes N and edges E. Under these assumptions, we focus on distinguishable packets undergoing random walks. The resulting dynamical equation for the total number of packets, Eq. (3), converges to a stationary state s^* when the packet generation rate g is below some critical value g_c given in Eq. (5). Both s^* and the throughput F given in Eq. (6) grow monotonically with respect to generation rate g in this range. Then, at some critical generation $g = g_c$, jamming emerges. In other words, as $g \to g_c^-$, the only fixed point s^* diverges to infinity, effectively resulting in the absence of stationary states. Thus, the total number of packets diverges to infinity, and the system is guaranteed to fail at some point, which is represented as the vanishing stationary throughput in our equations and figures. Moreover, the congestion appears abruptly and without apparent early-warning signals, resulting in a functionality loss of the network that is hard to anticipate. This mean-field theoretic conclusion is robust, extending to more complicated routing strategies, and to sparse and empirical network structures alike. Although mean-field theory predicts the critical generation rate accurately for relatively dense networks, it fails for sparse networks (see Fig. 1).

B. Network profiles and flow bottlenecks

The mesoscopic field theory approach aggregates topological information that specific nodes are regarded as similar with respect to their contribution to the flow properties, allowing us to compute quantitatively accurate results for realistic network structures beyond mean-field theory.

We organize the network in layers around a central node, where the neighbors of the center belong to the first layer, second neighbors are in the second layer, and so on.

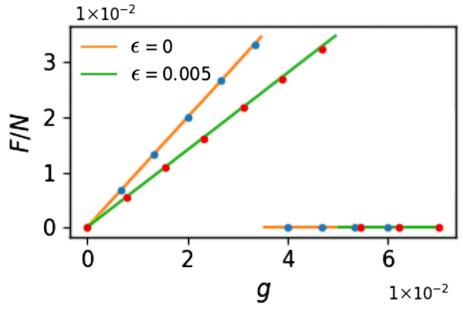

FIG. 5. Stationary throughput per node F/N as a function of generation rate g for distinguishable packets following random walks on a random three-regular network of $N = 50$ nodes. Two curves show the conservative ($\epsilon = 0$) and dissipative ($\epsilon = 0.005$) cases. The analytic curves are calculated using the mesoscopic field theory, Eq. (B2). Each marker comes from a single simulation.

The most relevant structural information for the central node is the number of nodes in each layer and interlayer and intralayer connectivities. We call this distilled structural information the network profile, as seen from a specific center. Defining the dynamical equations on these profiles allows us to accurately model the flow of randomly routed packets on networks with realistically sparse topologies where mean-field theory fails, compare Fig. 5 with Fig. 1(b).

The network profiles encode important information about the network by keeping the resolution high near the center and aggregating the data considerably in faraway regions. Predicting the unsustainability transition point, when the flow becomes unstable, relies on accurately modeling the flow near the bottlenecks, and this is where one needs the highest resolution. We find that describing the flow from the perspective of sinks is most accurate for distinguishable packets, while describing the flow from the perspective of sources is most accurate for interchangeable (i.e., indistinguishable) packets. This finding suggests that the bottlenecks tend to be near the sinks for distinguishable packets and near sources for interchangeable packets, which could provide insights for network resource provisioning, such as the optimal ratio of sources to sinks.

C. Dissipation can enhance throughput

The mesoscopic field theory approach also lets us uncover the fact that dissipation can counterintuitively enhance throughput in some circumstances. As shown in Fig. 5, introducing dissipation into the flow has two separate effects. First, nonzero dissipation implies that not all the generated packets make it through the network with some fraction dissipated on the way, thus reducing the throughput. This case is reflected as reduced slopes in the sustainable flow phase as shown in Fig. 5. On the other hand, dissipation reduces the total number of packets flowing on the network, and hence sustaining the flow

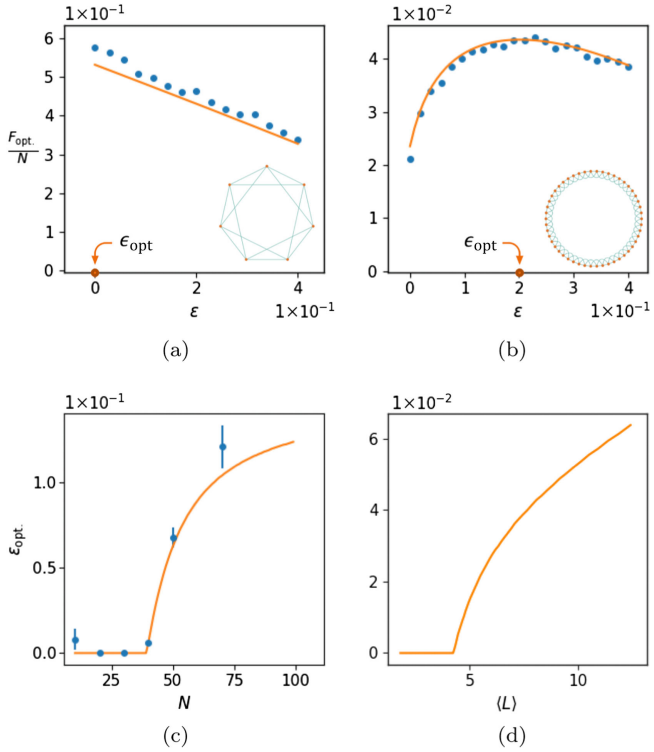

FIG. 6. Effects of dissipation on the flow. In the top row, we show stationary optimal throughput $[(F_{opt.})/(N)]$ as a function of dissipation ϵ for randomly routed distinguishable packets on small $N = 7$ (a) and large $N = 50$ (b) ring lattices with degree 4 (shown as insets). Each simulated data point is obtained by sweeping over the generation rates and identifying g_c, producing the optimal throughput F_{opt} for a fixed value of ϵ. The analytic curves are calculated using the mesoscopic field theory. In the bottom row, we show the optimal amount of dissipation ϵ_{opt} as a function of network size N for ring lattices with degree 10 (c) and ϵ_{opt} as a function of the mean shortest-path length $\langle L \rangle$ for a ring lattice with $N = 1000$ and variable lattice degree (d). The analytic curves are calculated using the mesoscopic field theory. The data points in panel (c) are obtained from simulations with three-dimensional parameter sweeping (ϵ, g, N).

becomes easier, resulting in delayed unsustainability transitions in Fig. 5. Thus, we are prompted to ask if there are certain symmetries (i.e., interchangeable versus distinguishable packets) and packet conservation laws for which dissipation can improve the optimal amount of stationary throughput.

We find that dissipation can indeed be useful for the flow of distinguishable packets. The top row of Fig. 6 shows the optimal amount of throughput (i.e., the height of the peak in Fig. 5) as a function of dissipation ϵ for randomly routed packets on small [Fig. 6(a)] and large [Fig. 6(b)] ring lattices. We see clearly that dissipation has a negative effect on the flow for the small lattice, while for the large lattice, the optimal throughput reaches the maximum for some nonzero dissipation ϵ_{opt}. Notice, moreover, that the solid lines in Figs. 6(a) and 6(b) represent our analytic results for

the optimal throughput for each given value of ϵ. Thus, the maximum of this graph pinpoints the optimal operation regime of the system in the two-dimensional parameter generation-dissipation (g, ϵ) space. Notably, the calculation depends only on the network structure.

Intuitively, the usefulness of dissipation comes from the fact that, for large enough networks, some fraction of the packets are lost far away from their destinations. The buildup of such packets jams the network unnecessarily, preventing other packets from reaching their destinations. Dissipation decreases the number of such lost packets and frees up the conduction capabilities of the network to maintain the flow. This effect does not occur in small networks, as seen in Fig. 6(a), because there is not enough space for packets to get lost, which has been known in the engineering community. In fact, the Internet Protocol incorporates dissipation through its so-called "time-to-live" mechanism and takes advantage of this phenomenon [55]. Here, we provide a first-principle derivation of this mechanism. Mathematically, the role of this type of dissipation has been addressed in simple settings through the so-called stochastic resetting paradigm [56,57], yet in networked topologies, the problem remains under-researched [58,59].

The above-described mechanism does not apply to flows of interchangeable packets. Any sink is a legitimate target for each packet. Hence, the buildup of lost packets is not a significant issue, and there is no benefit to introducing dissipation. Indeed, for all the numerical experiments and analytical computations, the optimal value of dissipation we observe is always $\epsilon_{\text{opt}} = 0$.

The possible existence of an optimal dissipation naturally leads us to inquire how this phenomenon emerges. In Fig. 6(a), we show the dependence of the optimal dissipation ϵ_{opt} on the network size N for ring lattices with fixed degree. We find that ϵ_{opt} is exactly 0 until a continuous transition occurs, after which it becomes positive; i.e., dissipation helps to maximize throughput. An alternative way to visualize this case is to keep the network size constant and vary the lattice degree instead so that the average shortest-path length $\langle L \rangle$ is modified accordingly. We observe again in Fig. 6(b) a continuous transition separating the phases in which dissipation is detrimental ($\epsilon_{\text{opt}} = 0$) and beneficial ($\epsilon_{\text{opt}} \neq 0$) for the throughput, which confirms the intuition mentioned above that when the average distance between the origin and destination becomes larger, the chance of a packet getting lost and congesting the system increases. Hence, a nontrivial amount of dissipation fixes this situation.

The three-dimensional parameter sweeping required to obtain these results from simulations is computationally very demanding. For this reason, in Fig. 6(b), we only present the curves from the analytic results. By relaxing this limiting factor, we can consider much larger networks ($N = 1000$), showcasing the advantage of the analytic approach in front of the computational experiments.

D. Effects of routing randomness

The full-scale field theory approach lets us consider routing strategies beyond random walks that take into account topological information. We have introduced the flow temperature T to interpolate between the shortest-path $T = 0$ and random-walk $T = 1$ routing. The effect of the routing temperature on the throughput F is presented in Fig. 7(a). When the temperature is increased, packets start wandering more and more and thus become dissipated more easily, resulting in reduced throughput. In some cases, increasing the temperature too much may result in an unsustainability transition, with the throughput reaching 0 in an abrupt manner.

An interesting scenario arises in some networks with rare, long-range connections, where nonzero temperature can actually prove itself useful. Such examples include

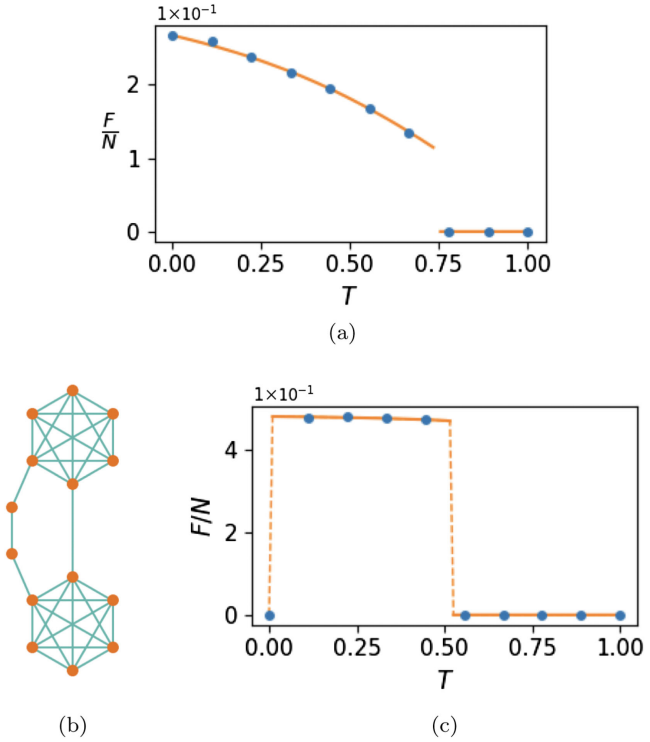

FIG. 7. Effect of smart routing strategies. In panel (a), we show the throughput per node (F/N) as a function of routing temperature T for distinguishable packets on a random three-regular network of $N = 50$ nodes with dissipation $\epsilon = 0.1$ and generation rate $g = 0.4$. The left edge, with $T = 0$, corresponds to the shortest-path routing, while the right edge, with $T = 1$, corresponds to the random walk. In panel (b), we show a toy network with two strong communities and two bridges between them: one long, one short. Panel (c) shows the throughput per node (F/N) as a function of routing temperature T for distinguishable packets on the graph in panel (b), with dissipation $\epsilon = 0.01$ and generation rate $g = 0.5$. The dash indicates the two transitions at $T = 0$ and $T > 0$. In all cases, each marker comes from a single simulation, and the analytic curves are calculated using the full-scale field theory.

modular [60] or small-world networks [61]. For simplicity, let us imagine a network with two strong communities and two bridges between them: one long and the other short [see Fig. 7(b)]. When the temperature is 0, all the packets traveling to the other community will try to squeeze through the short bridge, creating a jam and potentially making the flow unsustainable. Increased temperature, on the other hand, allows the packets to sample other trajectories, and some will end up using the long bridge, effectively increasing the throughput and potentially keeping the flow sustainable. Thus, the dependence of throughput on the routing temperature can have two unsustainability transitions, segmenting the figure into three phases where only the middle one can sustain the flow [see Fig. 7(c)].

Counterintuitively, the lower unsustainability transition turns out to be degenerate, in the sense that it occurs at exactly $T = 0$ as seen in Fig. 7(c). Suppose the flow is sustainable at some $T > 0$ but not at $T = 0$. Thus, at $T = 0$, the flow is not utilizing the full conductive potential of the network, and the total number of packets diverges. Increasing T slightly causes a very small fraction of these packets to choose the longer bridge, but since there were arbitrarily many packets, this small fraction is enough to utilize the full conductive potential of both bridges. Hence, the flow becomes sustainable for arbitrarily small nonzero temperatures. This effect is caused by our assumption that the node capacities are finite but arbitrarily large. In real-world scenarios, of course, the capacities are bounded, and if $T = 0$ results in an unsustainable system, one will need to increase it to some positive finite value until the flow becomes sustainable.

As a last point, we highlight that the full-scale theory is able to predict properties of flow with smart routing strategies even in empirical networks, which are characterized by complicated topological correlations. This capability is natural since, in our analytical derivations, we do not explicitly assume that the topologies need to be uncorrelated. In particular, we verify the accuracy of the theory by considering the problem of the flow of cars on the real road network of Chesapeake, Virginia [62] (see Fig. 8). In this case, cars are taken as distinguishable packets, and dissipation is set to 0 because they do not disappear. Car trajectories, in general, contain little randomness; thus, we set a low routing temperature of $T = 0.05$. The cars mostly follow the shortest-path trajectories to their destinations, yet the results are robust for other values of T.

E. Validation in empirical networks

As a last point, we showcase that our mesoscopic and full-scale theories can successfully predict flow properties on empirical networks, which is remarkable because real systems are characterized by complicated topological correlations that are generally difficult to handle in the description of dynamical processes on interconnected structures [60,63,64]. However, in our analytical derivations, we do not explicitly assume that the topologies need to be treelike or uncorrelated. In the mesoscopic treatment, interlayer connections can be seen as closed loops of arbitrary length that are explicitly considered in the theory. In the full-scale case, the two main key quantities our equations depend on are the adjacency matrix and the shortest-path tensor, which encode all the topological correlations present. Hence, we overcome the treelikeness assumption of current methods that offer only a baseline for comparison and fail to accurately predict the behavior of dynamical systems on actual empirical networks.

To illustrate our point, we focus on two applications in which the different symmetries, conservation laws, and

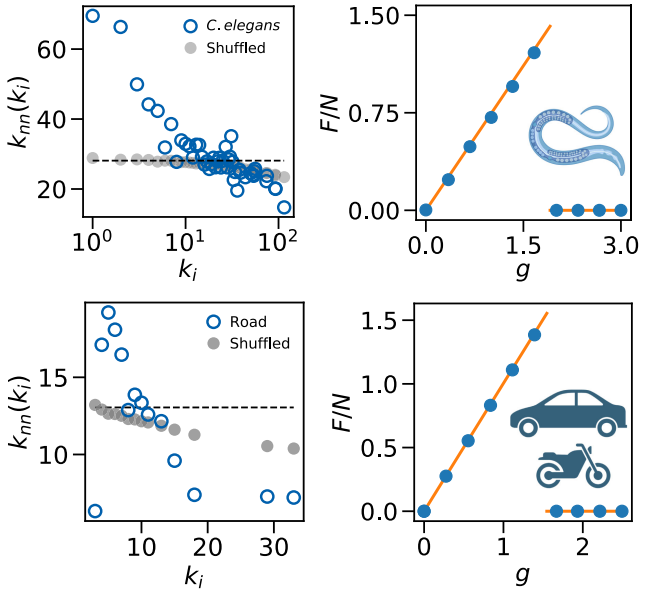

FIG. 8. Validation of the multiscale field theory in empirical networks. On the left column, we show the correlation patterns through the average degree of the neighbors of nodes of degree k_i for the actual empirical system and its randomized (shuffled) version. The horizontal dashed line is the theoretical value $\langle k^2\rangle/\langle k\rangle$. On the right, we show the stationary throughput per node F/N as a function of generation rate g. The considered applications are the dissipative flow of indistinguishable synaptic transmissions in the *C. elegans* connectome [66–69] (top row) and the conservative flow of distinguishable vehicles on a road network in Chesapeake, Virginia [62] (bottom row). For the *C. elegans*, one-third of the nodes are randomly assigned as designated sources (acting as sensory neurons), and another third are chosen as designated sinks (acting as motor neurons). The dissipation probability is chosen nominally as $\epsilon = 0.1$. The orange solid curve is the result of numerically finding the stationary states of the mesoscopic field-theoretic equations (13). Each marker comes from a single simulation. For the road network, we assume that vehicles do not dissipate and that they mostly follow the shortest paths; therefore, in both simulations (the markers) and full-scale field theory (solid line) a low routing temperature $T = 0.05$ is set. We have verified that the accuracy is maintained for other values of T. The theoretical line for the full-scale theory is retrieved from Eq. (17).

routing strategies discussed here apply: the *C. elegans* connectome and a road network (top and bottom rows of Fig. 8, respectively). We first verify that neither network is uncorrelated by computing $k_{\mathrm{nn}}(k_i)$, the average degree of the neighbors of nodes of degree k_i. For the *C. elegans*, $k_{\mathrm{nn}}(k_i)$ displays a decaying trend that indicates a disassortative connectivity pattern (Fig. 8, top left), while the road network exhibits a more complex structure, with a positive correlation for low degree nodes and a negative correlation for intermediate-to-large degree nodes (Fig. 8, bottom left). If these networks were to be uncorrelated and satisfy the requirement that the degree of the largest hub $k_{\max} \lesssim \sqrt{N}$, then $k_{\mathrm{nn}}(k_i)$ would be a constant equal to $\langle k^2\rangle/\langle k\rangle$. Actually, we observe that when we randomize the topology of these networks, $k_{\mathrm{nn}}(k_i)$ is not constant but decays with k_i, corresponding to the so-called structural disassortative phenomenon [65]. This phenomenon is induced by the fact that $k_{\max} > \sqrt{N}$, which further demonstrates the nontrivial organization of these empirical systems.

Regarding transport properties, we assume dissipative, diffusive flow of indistinguishable synaptic transmissions in the *C. elegans* brain network and conservative flow of distinguishable vehicles on the road network. We investigate the stationary throughput per node F/N as a function of generation rate g, verifying that, in both cases, the mesoscopic and full-scale theories provide excellent approximations for this metric (Fig. 8, right column). The jamming transition appears in an abrupt manner here as well, indicating that its discontinuity is not an artifact of the uncorrelated nature of networks. Overall, these results underscore the usefulness of our multiscale theory to accurately predict the behavior of network flow in empirically relevant applications under a variety of scenarios.

IV. CONCLUSIONS

The study of flow on complex networks spans diverse domains, from transportation and power grids to biological and information systems. Such a breadth of realms has led to conceptual differences in the modeling attempts of flows, often shaped by domain-specific applications. Therefore, the scarce, existing analytical approaches have remained divided, while computational approaches have been tailored to specific systems. This separation, in turn, has hindered the development of a unified, comprehensive framework capable of addressing big-picture questions regarding the effects and influences of various symmetries, conservation laws, and routing strategies, ultimately limiting our ability to design, optimize, and control these systems in an effective manner.

To address this challenge, we have developed a hierarchy of field-theoretic methods capable of modeling flows on networks characterized by various symmetries, conservation laws, and routing strategies. We provide three levels of description. Through a mean-field approach, we qualitatively describe the transition at which the flow becomes unsustainable when the demand exceeds the network's capacity. This transition is very robust and appears in all the cases considered, irrespective of the network substrate on which the flow unfolds. However, for sparse networks, we need to go beyond mean-field treatment to capture the critical point at which the flow is not sustainable anymore.

The mesoscopic field theory developed herein, based on the concept of network profiles, allows us to calculate this threshold accurately, accounting for the structure of underlying networks in the case of random-walk routing. It also unveils the role of dissipation, showing that dissipation reduces the maximum sustainable throughput for interchangeable packets. However, dissipation can be beneficial and can enhance throughput for distinguishable packets. Its optimal value becomes nonzero through a continuous transition as the mean path length in the network increases. The benefit of dissipation for distinguishable packets routed on large networks has been implicitly known by the engineering community for some time, such as the TCP/IP where packets disappear once they time out. Here, we provide a first-principles derivation, showing the underlying mechanism that the benefits of dissipation result from removing lost packets. Another notable aspect of the mesoscopic field theory is that the network profiles encode structural information about the network, keeping resolution high near the center and aggregating with distance from the center, which offers insights into the locations of bottlenecks, revealing that bottlenecks tend to be near sources for interchangeable packets and near sinks for distinguishable packets. This feature may provide insights for network design or smart routing protocols. We validate the mesoscopic approach on dissipative, diffusive flows of indistinguishable synaptic transmissions from sensory to motor neurons in the *C. elegans* brain network. This approach shows how the theory captures critical flow thresholds and bottleneck formation in a real biological system.

The full-scale field theory provides the most fine-grained description and enables the analysis of routing algorithms. We consider the spectrum of strategies from random diffusion to shortest-path routing by introducing a parameter called routing temperature, T, which controls the amount of randomness in the packet trajectories. We observe that an increase in the temperature may result in an unsustainability transition. We also find that in networks with specific kinds of long-range connections, like modular or small-world networks, a small amount of randomness in the packet trajectories can be beneficial for the throughput. Understanding if the spectral properties of a network can predict optimal levels of routing randomness is an outstanding problem. We validate the full-scale approach on the Chesapeake, Virginia road network, modeling the conservative flow of distinguishable cars primarily following shortest paths. The strong agreement between theory and simulation demonstrates the full-scale framework's

versatility in capturing demand-induced overload and routing effects.

The routing strategies discussed in this work employ information about the network topology in two contrasting ways. Indeed, random routing, which has $T = 1$, assumes no knowledge of the connectivity, apart from the direct contacts of a node, which are the locations where the packets can be transported. As soon as the routing temperature becomes less than 1, a global knowledge of the connectivity is required to perform the shortest-path moves, even if they occur very rarely for large T. Yet, accessing the complete topology can be informationally very costly, or even impossible, depending on the application domain. To overcome this challenge, intermediate navigation strategies, where only partial topological information is employed, may be desirable. This approach comprises, for instance, the case in which packets wander randomly up to reaching a node that is a certain number of hops away from the destination, after which a shortest-path protocol is implemented [47,70]. We highlight that our framework is flexible and can accommodate these more convoluted strategies as well, by simply combining the equations of the mesoscopic and full-scale theories on the corresponding subsets of nodes, once the origin and destination are identified. In fact, a huge advantage of our mathematical approach is that it does not rely on the common treelike assumption employed by many methods addressing network dynamics. Instead, we accomplish this either by explicitly incorporating intrashell connections into the profiles (Sec. II C) or by directly utilizing the adjacency matrix and the shortest-path tensor (Sec. II D). By removing the treelike assumption, we hope that the methods developed here will provide solid theoretical grounds for understanding a broader range of dynamical processes on networks.

In any case, the introduced multiscale theoretical framework can be easily further adapted to more particular scenarios relevant to network flows, such as incorporating nodes with finite capacity, making the node capacities and edge conductances heterogeneous, or exploring dynamic routing protocols. Similarly, an interesting research question that we have not addressed in the present work is the relationship between the flow properties with other network structural measures, e.g., k-core, betweenness centrality, or spectral properties. This approach would allow us to better understand the emergence of bottlenecks, thus identifying, in a more refined manner, key critical properties of nodes and links that can threaten the harmonious functioning of the network. Another line that may be worth exploring is the ability of our framework to unravel flow characteristics occurring in quantum networks, where the indistinguishability setting predominates [71–74]. Finally, we have assumed throughout that the topology is static. In empirical settings, though, sometimes this is not an accurate representation, and a dynamic viewpoint becomes necessary [75,76]. This viewpoint includes allowing nodes and links to be present intermittently in the network due to, for instance, refractory periods after partial overloads, internal failures, or targeted interventions. These advancements would further enhance the applicability of the framework to a wider range of real-world systems and provide solid ground for an overarching theory of network flows.

ACKNOWLEDGMENTS

G. M. and R. M. D. gratefully acknowledge support provided by Army Research Award No. W911NF-23-1-0087; O. A. acknowledges financial support from the Spanish Ministry of Universities through the Recovery, Transformation and Resilience Plan funded by the European Union (Next Generation EU), and the University of the Balearic Islands; O. A. and A. D.-G. acknowledge support from the Spanish Grant No. PID2021-128005NB-C22, funded by MCIN/AEI/10.13039/501100011033 and "ERDF A way of making Europe," from Generalitat de Catalunya (2021SGR00856), and from the AccelNet-MultiNet program, a project of the National Science Foundation (Awards No. 1927425 and No. 1927418).

APPENDIX A: ENSEMBLE-BASED ANALYTICAL EXPRESSIONS FOR THE NETWORK PROFILES

In this appendix, we give the details on how to derive analytical expressions for the variables N_r, E_r, and D_r employed in the main equations of the mesoscopic field theory. The goal is to provide expressions that directly depend on the degree distribution of the network or its moments. Some of them are known, while others could not be found in the literature. We report all of them here for completeness.

Let the excess degree be the number of connections minus 1 of a node that has been reached by following an edge, and let q_k be the excess degree distribution. It reads $q_k = (k+1)p_k/\langle k\rangle$, where $\langle k\rangle$ is the mean degree of p_k [42]. The average number of second neighbors is given by the average excess degree, $(\langle k^2\rangle - \langle k\rangle)/\langle k\rangle$, times the mean degree, i.e., $N_2 = \langle k^2\rangle - \langle k\rangle$. One can generalize these results by noting that the average number of nodes at layer r is the average number of nodes at the previous layer $r-1$ times the average excess degree, i.e.,

$$N_r = \left[\frac{\langle k^2\rangle - \langle k\rangle}{\langle k\rangle}\right]^{r-1}\langle k\rangle. \tag{A1}$$

This equation is valid for $r > 0$, and we take $N_0 = 1$, by definition. For the α profile, we condition the branching process to have a source of degree k_0. The above reasoning can be repeated to obtain

$$N_r(k_0) = \left[\frac{\langle k^2\rangle - \langle k\rangle}{\langle k\rangle}\right]^{r-1}k_0. \tag{A2}$$

For treelike networks, the generating function of the interlayer connections E_r is known [77], yet, to the best of our knowledge, the probability distribution of E_r has not been reported before. Even if for our purposes (N_r, E_r, D_r) represent the mean values of their corresponding distribution, we illustrate next how to compute such a distribution.

Let $g_0(x) \equiv \sum_{k=0}^{\infty} p_k x^k$ be the degree generating function. The probability associated with the sum of the degrees of n random nodes follows $[g_0(x)]^n$ [77,78]. To see this case, let us discuss the cases for a low value of n, say, $n = 2$. We have

$$\begin{aligned}[g_0(x)]^2 &= \left[\sum_{k=0}^{\infty} p_k x^k\right]^2 = \sum_{j=0}^{\infty}\sum_{k=0}^{\infty} p_j p_k x^{j+k} \\ &= (p_0 p_0)x^0 + (p_0 p_1 + p_1 p_0)x^1 \\ &\quad + (p_0 p_2 + p_1 p_1 + p_2 p_0)x^2 + \cdots.\end{aligned}$$

The probability that the sum is 0 is equal to two extractions of 0-degree nodes, hence $p_0 p_0$. The probability that the sum is 1 is equal to the extraction of a 0-degree node and a 1-degree node (taking into account the order of the extraction), hence the coefficient of x^1. Following the same reasoning, the probability of obtaining a degree value m is equal to the sum of all products $p_j p_k$ such that $j + k = m$, which remains valid for larger values of n.

In the case of n being a random variable itself, we need to make some adjustments. The generating function of this distribution is the convolution $g_0(g_0(x))$. To see this case, let us expand

$$\begin{aligned}g_0(g_0(x)) &= \sum_{k=0}^{\infty} p_k [g_0(x)]^k \\ &= p_0 + p_1[g_0(x)] + p_2[g_0(x)]^2 + \cdots.\end{aligned}$$

Each term corresponds to the probability of having j degrees to sum (p_j) times the generating function associated with the sum of that number of degrees $[g_0(x)^j]$.

Let us denote by q_k^r the distribution of the sum of the excess degrees of the nodes in shell r. Assuming that the network is treelike, this is precisely the distribution of our variables E_r. Similarly, let $g^r(x) \equiv \sum_{k=0} q_k^r x^k$ stand for the generating function of this distribution. The simplest case is $r = 1$. We know that the excess degree of each individual node is distributed according to the excess degree distribution q_k. If the focal node has j neighbors—an event that occurs with probability p_j—then the sum of excess degrees will be distributed according to $[g_1(x)]^j$. Averaging over all the possible numbers of neighbors of the focal node, we obtain

$$\begin{aligned}g^{r=1}(x) &= p_0 + p_1[g_1(x)] + p_2[g_1(x)]^2 + \ldots \\ &= g_0(g_1(x)) = \sum_{k=0}^{\infty} q_k^{r=1} x^k. \end{aligned} \tag{A3}$$

Using similar arguments, the excess degree distribution at an arbitrary shell r will have, as a generating function,

$$g^r(x) = g_0(g_1(g_1(\ldots g_1(x)\ldots))) = \sum_{k=0}^{\infty} q_k^r x^k, \tag{A4}$$

where we have to compose r generating functions $g_1(x)$ with $g_0(x)$.

To obtain the values q_k^r, we follow a combinatorial approach. If we have two series $f_1(x) = \sum_{n=1}^{\infty} a_n x^n/n!$ and $f_0(x) = \sum_{n=0}^{\infty} b_n x^n/n!$, its composition $f_0(f_1(x)) \equiv \sum_{n=0}^{\infty} c_n x^n/n!$ can be written as [79]

$$f_0(f_1(x)) = b_0 + \sum_{n=1}^{\infty} \frac{x^n}{n!}\left(\sum_{k=1}^{n} b_k B_{n,k}(a_1, \ldots, a_{n-k+1})\right),$$

where

$$\begin{aligned}B_{n,k}(x_1, \ldots, x_{n-k+1}) \equiv \sum \frac{n!}{j_1!\ldots, j_{n-k+1}!}\left(\frac{x_1}{1!}\right)^{j_1} \\ \times \left(\frac{x_2}{2!}\right)^{j_2} \cdots \left(\frac{x_{n-k+1}}{(n-k+1)!}\right)^{j(n-k+1)}\end{aligned}$$

are the Bell polynomials. The indices in the sums are conditioned such that $j_1 + j_2 + \cdots + j_{n-k+1} = k$ and $j_1 + 2j_2 + 3j_3 \ldots + (n-k+1)j_{n-k+1} = n$. Using these relations, then, everything narrows down to identifying $f_0(x)$ with $g_0(x)$ and $f_1(x)$ with either $g_1(x)$ or successive compositions of $g_1(x)$.

We obtain q_n^r in a recursive manner. In the first layer, we target $g^{r=1}(x) = g_0(g_1(x)) = \sum_k q_k^{r=1} x^k$; hence, by means of Eq. (A5), we identify $q_0^{r=1} = p_0$ and

$$\begin{aligned}q_n^{r=1} &= \frac{1}{n!}\sum_{k=1}^{n} k! p_k B_{n,k}(1!q_1, \ldots, (k-n+1)!q_{k-n+1}) \\ &= \frac{1}{n!}\sum_{k=1}^{n} k! p_k B_{n,k}\left(\frac{1!2}{\langle k\rangle} p_2, \frac{2!3}{\langle k\rangle} p_3, \ldots,\right. \\ &\quad \left.\frac{(k-n+1)!(k-n+2)}{\langle k\rangle} p_{k-n+2}\right).\end{aligned} \tag{A5}$$

In the second layer, we target $g^{r=2}(x) = g_0(g_1(g_1(x))) = \sum_k q_k^{r=2} x^k$. Thus, in this case, $f_0(x) = g_0(x)$, so $b_n = n! p_n$, and $f_1(x) = g_1(g_1(x)) = \sum_k a_k^{r=2} x^k$. We first need to find $a_n^{r=2}$ from this latter composition. Since

$$\begin{aligned}g_1(g_1(x)) = q_0 0! + \sum_{n=1}^{\infty} \frac{x^n}{n!}\sum_{k=1}^{n} k! q_k B_{n,k}(1!q_1, 2!q_2, 3!q_3, \\ \ldots, (k-n+1)!q_{k-n+1}),\end{aligned} \tag{A6}$$

the coefficients read

$$a_n^{r=2} = \frac{1}{n!}\sum_{k=1}^{n} k! q_k B_{n,k}(1! q_1, 2! q_2, 3! q_3, \ldots, (k-n+1)! q_{k-n+1}). \tag{A7}$$

The final composition is then

$$g_0(g_1(g_1(x))) = p_0 0! + \sum_{n=1}^{\infty}\frac{x^n}{n!}\sum_{k=1}^{n} k! p_k B_{n,k} \times (a_1^{r=2}, \ldots, a_{n-k+1}^{r=2}), \tag{A8}$$

so the excess degree distribution in the second layer is $q_0^{r=2} = p_0$ and

$$q_n^{r=2} = \frac{1}{n!}\sum_{k=1}^{n} k! p_k B_{n,k}\left(a_1^{r=2}, a_2^{r=2}, \ldots, a_{n-k+1}^{r=2}\right). \tag{A9}$$

One can repeat the composition of excess degree generating functions an arbitrary number of times to obtain the expression of the distribution of layer r. After some lengthy algebra, we obtain $q_0^r = p_0$ and

$$q_n^r = \frac{1}{n!}\sum_{k=1}^{n} k! p_k B_{n,k}\left(a_1^r, a_2^r, \ldots, a_{n-k+1}^r\right), \tag{A10}$$

with

$$a_n^r = \sum_{k=1}^{n} k! q_k B_{n,k}\left(a_1^{r-1}, \ldots, a_{n-k+1}^{r-1}\right) \quad \text{for } r > 2, \tag{A11}$$

$$a_n^r = n! q_n \quad \text{for } r = 1, 2. \tag{A12}$$

Despite being a convoluted expression, we manage to write the distribution of the interlayer variables E_r in terms of the degree and excess degree distributions of the original network.

The final variable related to the network profiles is D_r, which can be seen as the sum of E_{r-1}, E_r, and a sort of clustering coefficient $\tilde{C}_r$ between the N_r nodes of layer r. By definition, $D_0 = E_0$. In treelike networks, the probability of observing triangles vanishes as $N \to \infty$. Therefore, we can expect a similar asymptotic behavior for $\tilde{C}_r$. The clustering coefficient is known to be [42]

$$C = \frac{1}{N}\frac{[\langle k^2\rangle - \langle k\rangle]^2}{\langle k\rangle^3}. \tag{A13}$$

The intralayer connections contributing to D_r can be seen as closed triangles between layers $r-1$ and r. At odds with the clustering coefficient, $\tilde{C}_r$ is not a normalized quantity; therefore, we need to rescale C with the multiplicative factor N_r, which leads to

$$\tilde{C}_r = \frac{1}{N}\left[\frac{\langle k^2\rangle - \langle k\rangle}{\langle k\rangle}\right]^{r+1}. \tag{A14}$$

For the center of an α profile with degree k_0, we obtain

$$\tilde{C}_r(k_0) = \frac{1}{N}\left[\frac{\langle k^2\rangle - \langle k\rangle}{\langle k\rangle}\right]^{r+1}\frac{k_0}{\langle k\rangle}. \tag{A15}$$

A final point to address is, given a network ensemble, up to which layer we should compute these quantities, i.e., where we should truncate the equations. This computation reduces to approximating the radius R of the network. Following Ref. [77], the radius is given by

$$R = \frac{\ln[\langle k\rangle + (N-1)(x-1)] - \ln(\langle k\rangle)}{\ln(x)}, \tag{A16}$$

where we introduce $x \equiv [(\langle k^2\rangle - \langle k\rangle)/(\langle k\rangle)]$ to lighten the notation. For an α profile with a central node with degree k_0, we find

$$R(k_0) = \frac{\ln[k_0 + (N-1)(x-1)] - \ln(k_0)}{\ln(x)}. \tag{A17}$$

APPENDIX B: MATRIX EQUATION FOR MESOSCOPIC ANALYSIS

In Sec. II C 1, we have reported the steps and approximations to simplify the steady state of Eq. (10) into a linear system of equations in the form $\boldsymbol{A}\cdot\boldsymbol{x} = \boldsymbol{e}$. To lighten the notation, we introduce the following structural constants:

$$a_r^\alpha \equiv 2E\cdot P_{\alpha,r}^{\text{out}}(1-\epsilon), \qquad c_r^\alpha \equiv 2E\cdot P_{\alpha,r}^{\text{in}}(1-\epsilon),$$
$$b_r^\alpha \equiv 2E\cdot(P_{\alpha,r}^{\text{in}} + P_{\alpha,r}^{\text{out}} + P_{\alpha,r}^{\text{loc}}\epsilon), \qquad d_r^\alpha \equiv \frac{N_r^\alpha}{N-1}, \tag{B1}$$

which depend on the profile properties, on the features of the flow, and on the global properties of the network. Written explicitly, the expression $\boldsymbol{A}\cdot\boldsymbol{x} = \boldsymbol{e}$ reads

$$
\begin{bmatrix}
-1 & c_1^0 & 0 & 0 & \cdots & 0 & 0 & & & & & & & & 0 \\
a_0^0 & -b_1^0 & c_2^0 & 0 & & 0 & 0 & & & & & & & & d_1^0 \\
0 & a_1^0 & -b_2^0 & c_3^0 & & 0 & 0 & & & & & & & & d_2^0 \\
\vdots & & & & \ddots & & \vdots & & & & 0 & & & & \vdots \\
0 & 0 & 0 & 0 & & c_{R^0-1}^0 & 0 & & & & & & & & d_{R^0-2}^0 \\
0 & 0 & 0 & 0 & & -b_{R^0-1}^0 & c_{R^0}^0 & & & & & & & & d_{R^0-1}^0 \\
0 & 0 & 0 & 0 & & a_{R^0-1}^0 & -b_{R^0}^0 & & & & & & & & d_{R^0}^0 \\
 & & & & & & & \ddots & & & & & & & \vdots \\
 & & & & & & & -1 & c_1^m & 0 & 0 & \cdots & 0 & 0 & 0 \\
 & & & & & & & a_0^m & -b_1^m & c_2^m & 0 & & 0 & 0 & d_1^m \\
 & & & & & & & 0 & a_1^m & -b_2^m & c_3^m & & 0 & 0 & d_2^m \\
 & & & & 0 & & & \vdots & & & & \ddots & & \vdots & \vdots \\
 & & & & & & & 0 & 0 & 0 & 0 & & c_{R^m-1}^m & 0 & d_{R^m-2}^m \\
 & & & & & & & 0 & 0 & 0 & 0 & & -b_{R^m-1}^m & c_{R^m}^m & d_{R^m-1}^m \\
 & & & & & & & 0 & 0 & 0 & 0 & \cdots & a_{R^m-1}^m & -b_{R^m}^m & d_{R^m}^m \\
0 & w^0 & w^0 & w^0 & \cdots & w^0 & w^0 & \cdots & 0 & w^m & w^m & w^m & \cdots & w^m & w^m & 0
\end{bmatrix}
\cdot
\begin{bmatrix}
s_0^0 \\ s_1^0/S \\ s_2^0/S \\ \vdots \\ s_{R^0-2}^0/S \\ s_{R^0-1}^0/S \\ s_{R^0}^0/S \\ \vdots \\ s_0^m \\ s_1^m/S \\ s_2^m/S \\ \vdots \\ s_{R^m-2}^m/S \\ s_{R^m-1}^m/S \\ s_{R^m}^m/S \\ g_c
\end{bmatrix}
=
\begin{bmatrix}
0 \\ 0 \\ 0 \\ \vdots \\ 0 \\ 0 \\ 0 \\ \vdots \\ 0 \\ 0 \\ 0 \\ \vdots \\ 0 \\ 0 \\ 0 \\ 1
\end{bmatrix}. \tag{B2}
$$

[1] M. E. J. Newman, *The structure and function of complex networks*, SIAM Rev. **45**, 167 (2003).

[2] B. Tadić, G. Rodgers, and S. Thurner, *Transport on complex networks: Flow, jamming and optimization*, Int. J. Bifurcation Chaos Appl. Sci. Eng. **17**, 2363 (2007).

[3] A. Barrat, M. Barthelemy, and A. Vespignani, *Dynamical Processes on Complex Networks* (Cambridge University Press, Cambridge, England, 2008).

[4] M. P. Kavanaugh, *Neurotransmitter transport: Models in flux*, Proc. Natl. Acad. Sci. U.S.A. **95**, 12737 (1998).

[5] H. Barbosa, M. Barthelemy, G. Ghoshal, C. R. James, M. Lenormand, T. Louail, R. Menezes, J. J. Ramasco, F. Simini, and M. Tomasini, *Human mobility: Models and applications*, Phys. Rep. **734**, 1 (2018).

[6] H. Abdi, S. D. Beigvand, and M. La Scala, *A review of optimal power flow studies applied to smart grids and microgrids*, Renewable Sustainable Energy Rev. **71**, 742 (2017).

[7] A. Callado, C. Kamienski, G. Szabó, B. P. Gero, J. Kelner, S. Fernandes, and D. Sadok, *A survey on internet traffic identification*, IEEE Commun. Surv. Tutor. **11**, 37 (2009).

[8] O. Artime, M. Grassia, M. De Domenico, J. P. Gleeson, H. A. Makse, G. Mangioni, M. Perc, and F. Radicchi, *Robustness and resilience of complex networks*, Nat. Rev. Phys. **6**, 114 (2024).

[9] W. J. Wouter Botzen, Olivier Deschenes, and Mark Sanders, *The economic impacts of natural disasters: A review of models and empirical studies*, Rev. Environ. Econ. Pol. (2019).

[10] M. A. Benevolenza and L. DeRigne, *The impact of climate change and natural disasters on vulnerable populations: A systematic review of literature*, J. Hum. Behav. Soc. Environ. **29**, 266 (2019).

[11] A. H. Sanstad, Q. Zhu, B. Leibowicz, P. H. Larsen, and J. H. Eto, Case studies of the economic impacts of power interruptions and damage to electricity system infrastructure from extreme events, Energy Markets and Policy Department, Lawrence Berkeley National Laboratory (2020).

[12] J. A. Lewis, *Assessing the Risks of Cyber Terrorism, Cyber War and Other Cyber Threats* (Center for Strategic & International Studies, Washington, DC, 2002).

[13] K. Park, Y.-C. Lai, L. Zhao, and N. Ye, *Jamming in complex gradient networks*, Phys. Rev. E **71**, 065105(R) (2005).

[14] R. Guimerà, A. Díaz-Guilera, F. Vega-Redondo, A. Cabrales, and A. Arenas, *Optimal network topologies for local search with congestion*, Phys. Rev. Lett. **89**, 248701 (2002).

[15] L. Zhao, Y.-C. Lai, K. Park, and N. Ye, *Onset of traffic congestion in complex networks*, Phys. Rev. E **71**, 026125 (2005).

[16] B. Tadić and S. Thurner, *Search and topology aspects in transport on scale-free networks*, Physica (Amsterdam) **346A**, 183 (2005).

[17] K. Hu, C. Liu, T. Hu, and Y. Tang, *Enhancing traffic capacity for scale-free networks by the one-way links*, J. Phys. A **43**, 175101 (2010).

[18] Y. Zhuo, Y. Peng, C. Liu, Y. Liu, and K. Long, *Traffic dynamics on layered complex networks*, Physica (Amsterdam) **390A**, 2401 (2011).

[19] D. Hu and D. Cai, *Adaptation and optimization of biological transport networks*, Phys. Rev. Lett. **111**, 138701 (2013).

[20] A. Solé-Ribalta, S. Gómez, and A. Arenas, *Congestion induced by the structure of multiplex networks*, Phys. Rev. Lett. **116**, 108701 (2016).
[21] A. Solé-Ribalta, S. Gómez, and A. Arenas, *A model to identify urban traffic congestion hotspots in complex networks*, R. Soc. Open Sci. **3**, 160098 (2016).
[22] P. Echenique, J. Gómez-Gardenes, and Y. Moreno, *Dynamics of jamming transitions in complex networks*, Europhys. Lett. **71**, 325 (2005).
[23] G. Yan, T. Zhou, B. Hu, Z.-Q. Fu, and B.-H. Wang, *Efficient routing on complex networks*, Phys. Rev. E **73**, 046108 (2006).
[24] X. Ling, M.-B. Hu, R. Jiang, R. Wang, X.-B. Cao, and Q.-S. Wu, *Pheromone routing protocol on a scale-free network*, Phys. Rev. E **80**, 066110 (2009).
[25] D. De Martino, L. Dall'Asta, G. Bianconi, and M. Marsili, *Congestion phenomena on complex networks*, Phys. Rev. E **79**, 015101(R) (2009).
[26] W.-X. Wang, Z.-X. Wu, R. Jiang, G. Chen, and Y.-C. Lai, *Abrupt transition to complete congestion on complex networks and control*, Chaos **19**, 033106 (2009).
[27] M. Tang, Z. Liu, X. Liang, and P. Hui, *Self-adjusting routing schemes for time-varying traffic in scale-free networks*, Phys. Rev. E **80**, 026114 (2009).
[28] S. Meloni and J. Gómez-Gardeñes, *Local empathy provides global minimization of congestion in communication networks*, Phys. Rev. E **82**, 056105 (2010).
[29] X. Ling, M.-B. Hu, R. Jiang, and Q.-S. Wu, *Global dynamic routing for scale-free networks*, Phys. Rev. E **81**, 016113 (2010).
[30] W. Huang and T. W. Chow, *Effective strategy of adding nodes and links for maximizing the traffic capacity of scale-free network*, Chaos **20**, 033123 (2010).
[31] H.-X. Yang, W.-X. Wang, Y.-C. Lai, Y.-B. Xie, and B.-H. Wang, *Control of epidemic spreading on complex networks by local traffic dynamics*, Phys. Rev. E **84**, 045101(R) (2011).
[32] W.-X. Wang, C.-Y. Yin, G. Yan, and B.-H. Wang, *Integrating local static and dynamic information for routing traffic*, Phys. Rev. E **74**, 016101 (2006).
[33] B. Piccoli and M. Garavello, *Traffic Flow on Networks* (American Institute of Mathematical Sciences, New York, 2006).
[34] C. d'Apice, S. Göttlich, M. Herty, and B. Piccoli, *Modeling, Simulation, and Optimization of Supply Chains: A Continuous Approach* (SIAM, Philadelphia, 2010).
[35] A. Bressan, S. Čanić, M. Garavello, M. Herty, and B. Piccoli, *Flows on networks: Recent results and perspectives*, EMS Surv. Math. Sci. **1**, 47 (2014).
[36] R. M. D'Souza, *Curtailing cascading failures*, Science **358**, 860 (2017).
[37] A. Tejedor, A. Longjas, D. A. Edmonds, I. Zaliapin, T. T. Georgiou, A. Rinaldo, and E. Foufoula-Georgiou, *Entropy and optimality in river deltas*, Proc. Natl. Acad. Sci. U.S.A. **114**, 11651 (2017).
[38] M. Šuvakov and B. Tadić, *Modeling collective charge transport in nanoparticle assemblies*, J. Phys. Condens. Matter **22**, 163201 (2010).
[39] E. Wonisch, J. Mensing, and A. Heuer, *Second-order mean-field approximation for calculating dynamics in Au-nanoparticle networks*, Phys. Rev. E **110**, 034103 (2024).
[40] M. E. Newman, *Assortative mixing in networks*, Phys. Rev. Lett. **89**, 208701 (2002).
[41] L. Peel, J.-C. Delvenne, and R. Lambiotte, *Multiscale mixing patterns in networks*, Proc. Natl. Acad. Sci. U.S.A. **115**, 4057 (2018).
[42] M. Newman, *Networks* (Oxford University Press, New York, 2018).
[43] J. P. Bagrow, E. M. Bollt, J. D. Skufca, and D. Ben-Avraham, *Portraits of complex networks*, Europhys. Lett. **81**, 68004 (2008).
[44] M. Boguñá, R. Pastor-Satorras, and A. Vespignani, *Cut-offs and finite size effects in scale-free networks*, Eur. Phys. J. B **38**, 205 (2004).
[45] Y.-X. Kong, G.-Y. Shi, R.-J. Wu, and Y.-C. Zhang, *k-core: Theories and applications*, Phys. Rep. **832**, 1 (2019).
[46] M. Ahmed, R. Seraj, and S. M. S. Islam, *The k-means algorithm: A comprehensive survey and performance evaluation*, Electronics **9**, 1295 (2020).
[47] B. Tadić, *Cyclical trends of network load fluctuations in traffic jamming*, Dynamics **2**, 449 (2022).
[48] M. Cameron and E. Vanden-Eijnden, *Flows in complex networks: Theory, algorithms, and application to Lennard–Jones cluster rearrangement*, J. Stat. Phys. **156**, 427 (2014).
[49] C. T. Kelley, *Iterative Methods for Linear and Nonlinear Equations* (SIAM, Philadelphia, 1995).
[50] H. Nishimori and G. Ortiz, *Elements of Phase Transitions and Critical Phenomena* (Oxford University Press, New York, 2011).
[51] A. Avena-Koenigsberger, X. Yan, A. Kolchinsky, M. P. van den Heuvel, P. Hagmann, and O. Sporns, *A spectrum of routing strategies for brain networks*, PLoS Comput. Biol. **15**, e1006833 (2019).
[52] A. Mishra, T. Wen, and K. H. Cheong, *Parrondo's paradox in network communication: A routing strategy*, Phys. Rev. Res. **6**, L012037 (2024).
[53] K. Françoisse, I. Kivimäki, A. Mantrach, F. Rossi, and M. Saerens, *A bag-of-paths framework for network data analysis*, Neural Netw. **90**, 90 (2017).
[54] T. H. Cormen, C. E. Leiserson, R. L. Rivest, and C. Stein, *Introduction to Algorithms* (MIT Press, Cambridge, MA, 2022).
[55] J. Postel, Internet protocol, Tech. Rep. (1981).
[56] M. R. Evans and S. N. Majumdar, *Diffusion with stochastic resetting*, Phys. Rev. Lett. **106**, 160601 (2011).
[57] M. R. Evans, S. N. Majumdar, and G. Schehr, *Stochastic resetting and applications*, J. Phys. A **53**, 193001 (2020).
[58] A. P. Riascos, D. Boyer, P. Herringer, and J. L. Mateos, *Random walks on networks with stochastic resetting*, Phys. Rev. E **101**, 062147 (2020).
[59] O. Artime, *Stochastic resetting in a networked multiparticle system with correlated transitions*, J. Phys. A **55**, 484004 (2022).
[60] S. Fortunato and M. E. Newman, *20 years of network community detection*, Nat. Phys. **18**, 848 (2022).
[61] D. J. Watts and S. H. Strogatz, *Collective dynamics of 'small-world' networks*, Nature (London) **393**, 440 (1998).

[62] R. A. Rossi and N. K. Ahmed, *The network data repository with interactive graph analytics and visualization*, in *Proceedings of the AAAI conference on artificial intelligence* (2015).

[63] G. T. Cantwell and M. E. Newman, *Message passing on networks with loops*, Proc. Natl. Acad. Sci. U.S.A. **116**, 23398 (2019).

[64] O. Artime, J. J. Ramasco, and M. San Miguel, *Dynamics on networks: Competition of temporal and topological correlations*, Sci. Rep. **7**, 41627 (2017).

[65] A.-L. Barabási, *Network Science* (Cambridge University Press, Cambridge, England, 2016).

[66] J. G. White, E. Southgate, J. N. Thomson, S. Brenner *et al.*, *The structure of the nervous system of the nematode Caenorhabditis elegans*, Phil. Trans. R Soc. B **314**, 1 (1986).

[67] B. L. Chen, D. H. Hall, and D. B. Chklovskii, *Wiring optimization can relate neuronal structure and function*, Proc. Natl. Acad. Sci. U.S.A. **103**, 4723 (2006).

[68] L. R. Varshney, B. L. Chen, E. Paniagua, D. H. Hall, and D. B. Chklovskii, *Structural properties of the Caenorhabditis elegans neuronal network*, PLoS Comput. Biol. **7**, e1001066 (2011).

[69] WormAtlas/WormWiring Project, https://www.wormatlas.org/images/NeuronConnect.xls.

[70] À. Arenas, A. Cabrales, L. Danon, A. Díaz-Guilera, R. Guimerà, and F. Vega-Redondo, *Optimal information transmission in organizations: Search and congestion*, Rev. Econ. Des. **14**, 75 (2010).

[71] K. Azuma, S. E. Economou, D. Elkouss, P. Hilaire, L. Jiang, H.-K. Lo, and I. Tzitrin, *Quantum repeaters: From quantum networks to the quantum internet*, Rev. Mod. Phys. **95**, 045006 (2023).

[72] J. Biamonte, M. Faccin, and M. De Domenico, *Complex networks from classical to quantum*, Commun. Phys. **2**, 53 (2019).

[73] A. Andreev, A. Balanov, T. Fromhold, M. Greenaway, A. Hramov, W. Li, V. Makarov, and A. Zagoskin, *Emergence and control of complex behaviors in driven systems of interacting qubits with dissipation*, npj Quantum Inf. **7**, 1 (2021).

[74] S. DiAdamo, B. Qi, G. Miller, R. Kompella, and A. Shabani, *Packet switching in quantum networks: A path to the quantum internet*, Phys. Rev. Res. **4**, 043064 (2022).

[75] P. Holme and J. Saramäki, *Temporal networks*, Phys. Rep. **519**, 97 (2012).

[76] N. Masuda and R. Lambiotte, *A Guide to Temporal Networks* (World Scientific, Singapore, 2016).

[77] M. E. Newman, S. H. Strogatz, and D. J. Watts, *Random graphs with arbitrary degree distributions and their applications*, Phys. Rev. E **64**, 026118 (2001).

[78] H. S. Wilf, *Generatingfunctionology* (CRC Press, New York, 2005).

[79] L. Comtet, *Advanced Combinatorics: The Art of Finite and Infinite Expansions* (Springer Science & Business Media, New York, 1974).